Kinetic analysis supporting multielectron reduction of oxygen in bismuth tungstate-photocatalyzed oxidation of organic compounds

Haruna Hori,[1] Mai Takashima,*[1,2] Mai Takase[3] and Bunsho Ohtani[1,2]

[1]Graduate School of Environmental Science, Hokkaido University, Sapporo 060-0810, Japan
[2]Institute for Catalysis, Hokkaido University, Sapporo 001-0021, Japan
[3]Graduate School of Engineering, Muroran Institute of Technology, Muroran 050-8585, Japan

Keywords Photocatalytic organics decomposition; Two-electron oxygen reduction; Radical chain reaction; Bi(tri)modal light-intensity dependence; Threshold light intensity; Effective particle size

ABSTRACT

Light-intensity dependence of the rate of carbon-dioxide liberation in the photocatalytic decomposition of acetic acid by bismuth tungstate particles suspended in an aqueous solution under aerobic conditions was measured by monochromatic photoirradiation using a monochromator (lower intensity < 20 mW) and high-intensity UV-LED (higher intensity < 300 mW). The light-intensity dependence of both flake ball-shaped micrometer-sized particles (FB-BWO) and wet ball-milled nanometer-sized particles (ML-BWO) seemed to be bimodal, i.e., first and 0.5th orders in the lower and higher intensity ranges, respectively. Approximately 1.5th and second-order light-intensity dependences were also observed for ML-BWO at the lowest intensity range and for FB at the highest intensity range, respectively. The light-intensity dependences could be reproduced by a kinetic model that was derived on the basis of the assumption of oxygen reduction via two-electron (and possibly four-electron at the highest intensity region) transfer and a radical chain mechanism with peroxy radicals as chain carriers. The calculated threshold intensity between the first and 0.5th-order light-intensity dependences for FB-BWO was appreciably lower than that of ML-BWO, suggesting that the higher FB-BWO activity is attributable to the larger effective particle size for accumulation of two (or four) electrons.

1. Introduction

Heterogeneous photocatalysis is one of the most promising technologies for advanced oxidation processes. It has been and will continue to be applied to practical processes for decomposition of various organic/inorganic compounds in water or air [1,2]. One of the significant merits of photocatalytic oxidation in practical applications is that the chemical processes do not necessarily cleave bonds of oxygen (O_2) molecules to produce oxygen active species, i.e., photocatalytic oxidation proceeds through positive-hole transfer and subsequent radical-chain

*corresponding author.
E-mail address: takashima.m@cat.hokudai.ac.jp (Mai Takashima)

reactions, and O_2 is just used for scavenging photoexcited electrons, as a counter part of hole-induced oxidation, and for capturing intermediate radical species to liberate peroxy radicals as chain carriers. It is well known that titania, the most frequently used photocatalyst, can reduce O_2 easily with photoexcited electrons [3,4]. In other words, high efficiency of titania-induced photocatalytic decomposition of organic compounds in air or water is guaranteed by the reduction of O_2 with photoexcited electrons, not by the oxidation ability of titania photocatalysts, since the valence-band top positions of almost all simple and mixed metal oxides seem to be the same [5,6]. Then, for other metal oxide photocatalysts that can also absorb visible light as well as ultraviolet light, i.e., having smaller band gaps, the conduction-band (CB) bottom position is appreciably low (anodically shifted) and thereby one-electron reduction of O_2 cannot proceed, resulting in their poor activity for decomposition of organic compounds.

We have recently reported [7,8] that bismuth tungstate (Bi_2WO_6; BWO), which has a relatively low CB-bottom position that is not sufficient to drive one-electron O_2 reduction, can drive efficient photocatalytic decomposition of organic compounds under visible-light irradiation through a mechanism of multielectron reduction of O_2. This was supported by the observed photocatalytic activity that depends strongly on the kind of substrate to be reduced by CB electrons, on the basis of the estimated CB-bottom position, i.e., thermodynamic evidence [9,10]. However, it was also observed that tungsten(VI) oxide (WO_3; tungstena), for which the CB-bottom position is also estimated to be insufficient to drive one-electron O_2 reduction, was activated only when loaded with platinum [11], tungsten-carbide [12], copper(II)-oxide [13] or copper oxide cluster [14] deposits as a catalyst for multielectron O_2 reduction. However, the thermodynamic evidence cannot exclude the possibility that BWO drives one-electron reduction, not multielectron reduction, of O_2 by an unknown mechanism.

In the discussion on such multielectron/positive hole processes in photocatalysis, there seemed to have been misunderstandings of its meaning. In order to check the ability for driving photocatalytic reactions, the CB bottom (or valence-band top) position of a photocatalyst material is compared with the standard electrode potential of a reaction substrate(s), the most important thermodynamic concept in electrochemistry. The number of electrons discussed here for multielectron/positive hole transfer is the number of electrons included in the definition of standard electrode potential. For example, standard electrode potentials for two-electron O_2 reduction ($O_2 + 2H^+ + 2e^- = H_2O_2$, 0.70 V vs SHE) [15] and four-electron O_2 reduction ($O_2 + 4H^+ + 4e^- = 2H_2O$, 1.23 V vs SHE) [15] assume an electrochemical equilibrium, i.e., forward and backward currents cancel out to be totally no current; at least two or four electrons must move both forward and backward in the former and latter electrochemical equilibria, respectively. In electrochemical systems, the number of transferred electrons (n) can be estimated by checking the actual electrode potential. For example, if the potential of an electrode for O_2 reduction is 1 V, a four-electron process, not a two-electron process, is presumed. However, such an electrode potential cannot be measured in photocatalytic reaction systems, and, before discussing the electrode potential, the presence of multiple electrons/positive holes to be transferred is not guaranteed. Thus, a thermodynamic approach may not give any answers for n.

There has been discussion in a few papers about the number *n* for O_2 multielectron reduction by measuring a possible intermediate(s). An example is detection of hydrogen peroxide (H_2O_2) as a product of two-electron reduction [16], but H_2O_2 can also be produced by one-electron reduction of O_2 ($O_2 + H^+ + e^- = HO_2•$, –0.05 V vs SHE) [15] followed by reduction of $HO_2•$ into H_2O_2. Furthermore, even if H_2O_2 is produced by one-electron or two-electron O_2 reduction, H_2O_2 may disappear due to the further reduction to water since its standard electrode potential ($H_2O_2 + 2H^+ + 2e^- = H_2O$, 1.78 V vs SHE) [15] is lower (more anodic) than that of a one-electron or two-electron O_2 reduction process [8].

Thus, proving the proposed multielectron O_2 reduction is challenging, since thermodynamic and product-analytical methods cannot exclude the other possibilities. Here, we present the kinetic evidence supporting further O_2 multielectron reduction in BWO photocatalysis. Although, of course, this cannot solve the problem of exclusion of other possible interpretations, discussion of the effects of BWO particle size and shape on photocatalytic activity with a newly developed kinetic model gives new insights into the mechanism that have not been proposed so far in the field of photocatalysis.

2. Experimental

2.1 Materials

Flake ball-shaped (FB) BWO micrometer-sized particles were prepared according to our previous reports through a hydrothermal reaction [8,17,18]. Briefly, a mixture of bismuth nitrate pentahydrate ($Bi(NO_3)_3·5H_2O$; 5.0 mmol) and sodium tungstate dihydrate ($Na_2WO_4·2H_2O$; 2.75 mmol = 10% molar excess) in 70 mL water was poured into a Teflon (PTFE) bottle and heated at 433 K for 20 h to obtain a light-yellow FB-BWO powder. Wet-milled samples were prepared using a planetary ball mill with zirconia beads and water as a solvent. After milling, the suspension was sonicated and stood still to separate the upper (ML) and lower (MH) parts, which were then recovered as powders. Parts of the thus-prepared FB, ML and MH samples were calcined at 773 K in air to obtain 500FB, 500ML and 500MH, respectively. For details, see SI.

2.2 Characterization of sample powders

The morphology and size of particles were analyzed by field-emission scanning electron microscopy (FE-SEM; Jeol JSM-7400F) operated in the mode of low secondary-electron image (LEI) with measurement parameters of 10.0-μA current, 10.0-kV electron-acceleration voltage and 6-mm working distance. A small amount of the sample powder was fixed on conductive carbon tape (Okenshoji #15-1096) on a brass sample stage (12 mm in diameter; 10 mm in height) and evacuated (< 100 Pa) overnight before measurement.

Diffuse reflection (DR) spectra of samples were recorded on a Jasco V-670 ultraviolet and visible spectrophotometer equipped with an integrating sphere unit. Barium sulfate ($BaSO_4$) was used as a reference.

2.3 Action spectrum and light intensity-dependence analysis

A 30-mg portion of a sample was suspended in a 5.0vol% aqueous solution (3.0 mL) of acetic acid in a quartz cell and irradiated under aerobic conditions using a diffraction grating-type illuminator (Jasco CRM-FD) equipped with a 300-W xenon lamp (Hamamatsu Photonics C2578-02). The intensity of monochromatic irradiation (ca. 15-nm accuracy) was measured by a Hioki 3664 light-power meter equipped with a 9742 light sensor to be in the range of ca. 2–4 mW. The liberated carbon dioxide (CO_2) was analyzed by a Shimadzu GC-8A gas chromatograph equipped with a TCD and a Porapak-Q column. Photocatalytic activity was evaluated as rate of CO_2 liberation, and apparent quantum efficiency was evaluated as the ratio of the rate (mol s^{-1}) to light flux (mol s^{-1}).

Light-intensity dependence of the photocatalytic reaction rate in a low intensity (< ca.10 mW) region was measured using the above-mentioned illuminator at the wavelengths of 320, 350, 380 and 410 nm. For high-intensity irradiation, a 365-nm UV-LED (NS-Lighting ULDEN-101) emitting maximally ca. 320 mW was used. Light intensity was measured as total power of light in the irradiated area (1-cm square) in units of mW. Except for the highest intensity region for the UV-LED irradiation (> 250 mW) in which the center part was high, irradiation seemed almost homogeneous and the measured intensity (mW) can be equal to that shown in the unit of mW cm^{-2}.

3. Results and Discussion

3.1 Structural and physical properties of BWO samples

Figure 1 shows FE-SEM images of the BWO samples used in this study.

(**Fig. 1** FE-SEM images of BWO samples. (a, b) FB, (c, d) 500FB, (e, f) ML, (g, h) 500 ML, (i, j) MH and (k, l) 500MH.)

As has already been reported [18,19], hydrothermal reaction of a mixture of bismuth nitrate and sodium tungstate leads to the formation of FB-BWO micrometer-sized particles with a hierarchical structure, i.e., spherical assembly of flakes of stacked crystallite plates. Wet milling of these FB-BWO particles decomposed the FB structure into nanometer-sized platelets, ML and MH-BWO; aggregates of those platelets might have been formed during the drying after wet milling. There seemed to be no difference between the morphology of ML and that of MH as far as can be seen in the images in **Fig. 1**. Calcination of these samples at 773 K in air did not lead to an obvious change in morphology; the flakes of FB became slightly thicker presumably due to fusion of the BWO plates to result in ca. 2-times lower specific surface area, as reported previously [8].

3.2 Comparison of photocatalytic activities under low-intensity monochromatic and polychromatic irradiation modes

Figure 2 shows plots of photocatalytic activities of BWO samples under low-intensity monochromatic photoirradiation (by a monochromator) as a function of activities under

polychromatic mercury-arc irradiation [20,21] (>ca. 290 nm; ca. 33 mW for total irradiation area of ca. 2.5 cm^2).

(**Fig. 2** Photocatalytic activities of BWO samples under monochromatic irradiation (closed circles, open circles and triangles corresponding to irradiation at 320, 350 and 365 nm, respectively) as a function of activities under polychromatic mercury-arc irradiation.)

The intensity of the monochromatic irradiation was in the range of several milliwatts, but there was a tendency for an almost proportional relation between the photocatalytic activities under monochromatic irradiation and polychromatic irradiation. As shown in Fig. S1, there was also a linear relation between photocatalytic reaction rate of CO_2 liberation from acetaldehyde in air and from acetic acid in water under aerobic conditions. Therefore, it is reasonable to use the present acetic-acid decomposition under monochromatic irradiation as a test reaction system for analysis of the fundamental mechanism of photocatalytic decomposition of organic compounds in the presence of O_2.

3.3 Diffuse reflectance and action spectrum analysis of BWO samples

DR spectra of BWO samples are shown in **Fig. 3**.

(**Fig. 3** DR and action spectra of (a) as-prepared FB, ML and MH samples and (b) 773 K-calcined 500FB, 500ML and 500 MH samples. For action spectra, apparent quantum efficiency standardized to be 100 at the wavelength of 320 nm was plotted as a function of the wavelength of monochromatic light.)

A shoulder was observed in the DR spectra of FB and 500FB samples in addition to the ordinary absorption onset at ca. 420–450 nm observed for ML, MH, 500ML and 500MH samples (In other words, DR spectra of FB and 500FB were red-shifted compared with those of the other samples.). If all of the BWO samples used in this study are composed of pure bismuth tungstate, such absorption would be due to structural color. However, no appreciable shoulder was observed in the action spectra of FB and 500FB samples (as discussed below), suggesting that the shoulder in DR spectra is an artifact without substantial photoabsorption by BWO. As discussed in the previous paper [8], one of the most probable reasons for the shoulder is an amorphous tungstena component possibly remaining in hydrothermally synthesized FB-BWO, not structural color such as multiple reflection of light incident vertically to the plates of FB-BWO particles, though such structural color in FB-BWO had been speculated [22]. As stated in the introduction of this paper, (amorphous) tungstena may have poor ability for photocatalytic decomposition of organic compounds and therefore a shoulder might not appear in the action spectra of FB and 500FB samples.

Although the action spectra for uncalcined milled samples (ML and MH) were scattered, due to a one-order of magnitude lower intensity compared with that of mercury-arc irradiation and relatively low photocatalytic activity, and not clear for onset wavelengths, the action spectra of all

BWO samples were similar in rough estimation and it is reasonable to assume that bandgap excitation of BWO drives photocatalytic acetic-acid decomposition under aerobic conditions.

On the basis of the physicochemical background of action-spectrum analysis of heterogeneous photocatalytic reactions [23,24], coincidence of (diffuse reflectance) absorption and action spectra, as for the above-mentioned BWO samples, suggests that quantum efficiency, i.e., efficiency of utilization of photoexcited electron-positive hole pairs, is independent of irradiation wavelength. In other words, in such a case, the observed rate of photocatalytic reaction is proportional to the light intensity, i.e., the order of light-intensity dependence is unity for photocatalytic oxidative decomposition of acetic-acid by the BWO samples. However, such first-order light-intensity dependence seems strange for photocatalytic oxidative decomposition of organic compounds under aerobic conditions because a radical chain reaction may be involved in the mechanism of photocatalytic processes leading to 0.5th light-intensity dependence [25–27].

3.4 Light-intensity dependence of photocatalytic reaction by BWO samples

Figure 4 shows plots of the wavelength dependence of apparent quantum efficiency and order of light-intensity dependence for BWO samples.

(**Fig. 4** Wavelength dependence of (upper) apparent quantum efficiency and (lower) light-intensity dependence order of BWO samples. Black, dark grey, light gray and white bars correspond to data at 320, 350, 380 and 410 nm, respectively. Figures in the upper panels correspond to photocatalytic activity measured under mercury-arc irradiation standardized to be 100 for FB.)

As discussed for the results shown in **Fig. 2**, the photocatalytic-activity trends under monochromatic irradiation were similar to those under mercury-arc irradiation; among uncalcined samples, FB exhibited the highest activity, while wet-milled samples (ML and MH) showed poor activity at any wavelength, and calcination enhanced the activity, especially for the milled samples to result in the highest activities among all six BWO samples [8]. Light-intensity dependence was measured in each set of monochromatic irradiation by changing the light intensity of maximally ca. 10 mW. The results are shown in the lower panels in **Fig. 4**. The order of light-intensity dependence was almost equal to or slightly lower than unity in almost all cases, as had been predicted by the above-mentioned action-spectrum analysis (**Fig. 3**) using similar low-level light intensity. Exceptions were the light-intensity dependence of ML and that of MH under irradiation of 320 and 350 nm and the order was in the range of 1.3–1.5. Again, such a light intensity-dependence order higher than unity suggested a complexed mechanism, probably including higher-order light intensity-dependence processes, that is different from those in titania-photocatalyzed decomposition of organic compounds.

Figure 5 shows double-logarithmic plots of the reaction rate and light intensity observed in the FB or ML-photocatalyzed acetic-acid decomposition under highly intense 365-nm UV-LED photoirradiation.

(**Fig. 5** Double-logarithmic plots of the reaction rate (R) and light intensity (I) observed in the FB or ML-photocatalyzed acetic-acid decomposition under highly intense 365-nm UV-LED photoirradiation (open circles). Data obtained by a diffraction grating-type illuminator are also plotted; closed triangles, circles and squares correspond to irradiation wavelengths of 320, 350 and 380 nm.)

Approximate orders of light-intensity dependence estimated from the slope of lines are shown by triangles. Although the rates by those two BWO samples at the same intensity were different, both light-intensity dependences seemed to be trimodal; it is possible to see that FB and ML exhibited changes of approximate light-intensity dependence order of 1–0.5–2 and 2–1–0.5, respectively, with increase in light intensity. The second-order light-intensity dependence at the highest and lowest intensity regions for FB and ML, respectively, seemed uncertain, but an order higher than unity could be observed. This higher order light-intensity dependence of ML at the lowest intensity region may correspond to the 1.3–1.5th order in **Fig. 4**. The change of light intensity-dependence order 1–0.5 was commonly observed, and threshold intensities (I_{thr}) of this change of order were ca. 4 and 80 mW for FB and ML, respectively (Even when no change in the order at ca. 80 mW for ML was assumed, it could be said that I_{thr} for ML was appreciably higher than that for FB.). The bimodal 1–0.5th order and difference in I_{thr} depending on the kind of photocatalyst may be the key for understanding BWO-induced photocatalysis kinetics.

3.5 Kinetic model reproducing bimodal (trimodal) light-intensity dependence

The kinetic model proposed here includes two fundamental assumptions. One assumption is a radical chain reaction for decomposition of the reaction substrate (RH) with peroxy-radical (RO_2•) chain carriers and the other assumption is the necessity of successive accumulation of electrons in one BWO particle (<BWO>); a one electron-bearing particle (<BWO(1e)>) is produced by the reaction of a positive hole and RH, but it is assumed to undergo a backward reaction to disappear unless the second electron is created within the lifetime of <BWO(1e)> to give a two electron-bearing particle (<BWO(2e)>), which reduces O_2 by two-electron transfer. In other words, one electron-bearing BWO (actually <BWO(1e)-R•>) does not have sufficient ability to reduce O_2 in a one-electron reduction mode, and <BWO(2e)> can release R• accompanied by two-electron reduction of O_2. Therefore, based on the assumption that <BWO(1e)> has a very short life time and a positive hole that has been transferred to RH does not contribute to practical consumption of RH, only <BWO(2e)> produces R• for the overall reaction. For simplicity, deactivation of < BWO(2e)> to <BWO> or <BWO(1e)> and change in O_2 (surface) concentration are neglected. The reactions involved in BWO photocatalysis are as follows.

(reaction step)	(rate)	(description)	
<BWO> + $h\nu$ → <BWO(1e)>	$I\psi_0\phi$	first excitation	(1)
<BWO(1e)> + $h\nu$ → <BWO(2e)>	$I\psi_1\phi$ [BWO(1e)]	second excitation	(2)
<BWO(1e)> → <BWO>	k_d [BWO(1e)]	deactivation	(3)
<BWO(2e)> + RH → <BWO> + R•	k_r [BWO(2e)][RH]	radical formation	(4)

$R\bullet + O_2 \rightarrow RO_2\bullet$	$k_i\,[R\bullet][O_2]$	initiation	(5)
$RO_2\bullet + RH \rightarrow RO_2H + R\bullet$	$k_p\,[RO_2\bullet][RH]$	propagation	(6)
$2RO_2\bullet \rightarrow RO_4R$	$k_t\,[RO_2\bullet]^2$	termination	(7)

where I, ψ_0, ψ_1, ϕ and k's are light intensity, absorption efficiency of <BWO>, absorption efficiency of <BWO(1e)> and rate constants, respectively. The efficiency of excitation to create an electron-positive hole pair, ϕ, can be assumed to be the same for <BWO> and <BWO(1e)>, since the efficiency depends predominantly on the properties of BWO, while photoabsorption coefficients, ψ_0 and ψ_1, may be different, since ψ_0 depends predominantly on the bulk composition, i.e., photoabsorption coefficient of BWO, but ψ_1 must depend also on the effective size of a particle, as discussed later.

By applying steady-state approximation to <BWO(1e)>, <BWO(2e)>, R• and RO_2• (d[BWO(1e)]/dt = d[BWO(2e)]/dt = d[R•]/dt = d[RO_2•]/dt = 0), the following equations are derived.

$$[\mathrm{BWO(1e)}] = I\psi_0\phi / (k_d + I\psi_1\phi) \quad (8)$$

$$[\mathrm{BWO(2e)}] = I^2\psi_0\psi_1\phi^2 / k_r[\mathrm{RH}](k_d + I\psi_1\phi) \quad (9)$$

$$k_r[\mathrm{BWO(2e)}][\mathrm{RH}] = k_i[\mathrm{R}\bullet][\mathrm{O_2}] - k_p[\mathrm{RO_2}\bullet][\mathrm{RH}] \quad (10)$$

$$k_t[\mathrm{RO_2}\bullet]^2 = k_i[\mathrm{R}\bullet][\mathrm{O_2}] - k_p[\mathrm{RO_2}\bullet][\mathrm{RH}] = k_r[\mathrm{BWO(2e)}][\mathrm{RH}]$$
$$= I^2\psi_0\psi_1\phi^2 / (k_d + I\psi_1\phi) \quad (11)$$

$$[\mathrm{RO_2}\bullet] = \{I^2\psi_0\psi_1\phi^2 / k_t(k_d + I\psi_1\phi)\}^{1/2} \quad (12)$$

Then, overall rate (r) is obtained as,

$$r = -\mathrm{d[RH]/dt} = k_r\,[\mathrm{BWO(2e)}][\mathrm{RH}] + k_p\,[\mathrm{RO_2}\bullet][\mathrm{RH}]$$
$$= I^2\psi_0\psi_1\phi^2/(k_d + I\psi_1\phi) + k_p[\mathrm{RH}]\{I^2\psi_0\psi_1\phi^2 / k_t(k_d + I\psi_1\phi)\}^{1/2} \quad (13)$$
$$= I^2\psi_0\psi_1\phi^2/(k_d + I\psi_1\phi) + \alpha\{I^2 / (k_d + I\psi_1\phi)\}^{1/2}, \quad (14)$$

where $\alpha = k_p[\mathrm{RH}](\psi_0\psi_1\phi^2 / k_t)^{1/2}$. The first and second terms in **eq. 14** correspond to consumption of RH by direct positive-hole reaction and radical chain reaction, respectively, and the first term can therefore be neglected if the chain is sufficiently long (There seems to be no effective way to determine the chain length of a given chain reaction in photocatalysis, but a paper from the authors' group suggested that the first term could be small in photocatalytic acetic-acid decomposition by titania photocatalysts [27]). In such a case, the rates at lower and higher limits of light intensity (I) are derived as

$$r = \alpha' I \qquad (\text{when } k_d >> I\psi_1\phi,\ \alpha' = \alpha / k_d^{1/2}) \quad (15)$$

$$r = \alpha'' I^{1/2} \qquad (\text{when } k_d << I\psi_1\phi,\ \alpha'' = \alpha / (\psi_1\phi)^{1/2}), \quad (16)$$

reproducing the first and 0.5th-order light-intensity dependence shown in **Fig. 5**. Their threshold intensity (I_{thr}) is defined by assuming $\alpha' I = \alpha'' I^{1/2}$ to be k_d / ($\psi_1\phi$). This bimodal light-intensity dependence means that the probability of creation of <BWO(2e)>, requiring 2 photons, increased with square of light intensity at the lower intensity, but two-photon absorption by a BWO particle is guaranteed at an intensity higher than I_{thr}, and these second and first-order light-intensity dependences are multiplied by 0.5, the light-intensity dependence order for the part of the radical

chain reaction, to become first and 0.5th-order light-intensity dependences, respectively. The ca. 20-times lower I_{thr} of FB (ca. 4 mW) than that of ML (80 mW) can be explained by the larger effective size of FB, i.e., the larger crystalline-sized FB particles have a higher probability of absorption of the second photons to create <BWO(2e)> even if the constants k_d and ϕ are constant. As shown in **Fig. 6**, trimodal light-intensity dependence of FB could be presumed, though the data seemed rather scattered, and was shifted downward and change in I_{thr} was not obvious, suggesting that the effective particle size of FB remained almost constant even after calcination at 773 K.

(**Fig. 6** Double-logarithmic plots of the reaction rate and light intensity observed in the FB or 500FB-photocatalyzed acetic-acid decomposition under high-intensity 365-nm UV-LED photoirradiation.)

This seems consistent with the SEM observation shown in **Fig. 1**. The difference in overall photocatalytic activities depending on the kind of BWO sample (**Fig. 4**) can be interpreted, using this kinetic model, as follows. Assuming constant ψ_0, ϕ (for the same bulk composition of BWO samples) [RH], k_p and k_t (for the same reaction), the difference in the rate in the first-order light-intensity dependence region is attributed to the difference in k_d and ψ_1. At present, we have no information for the k_d, rate constant for deactivation (backward reaction) and cannot exclude the possibility of a k_d-dependent rate, but ψ_1 may be the key. Possible interpretations are: (1) decrease in photocatalytic activity by milling FB into ML/MH is due to a decrease in effective particle size to result in lower ψ_1 and (2) increase in photocatalytic activity by calcination of ML/MH is due to an increase in effective particle size by heat-induced aggregation of small particles.

In the above discussion, the first term in **eq. 14**, contribution of direct positive-hole reaction, is neglected, i.e., assuming a large chain length of the radical chain reaction. However, if the actual concentration of RO_2• ([RO_2•]) is high, the chain length is decreased, as suggested for titania photocatalysis by irradiation of a shorter wavelength [27]. The light intensity-dependence order of 1.3–1.5 for ML and MH samples when irradiated at 320 and 350 nm (**Fig 4**) and the lowest intensity part of ML light-intensity dependence (**Fig. 5**) is attributable to this shortened chain length due to a possible high concentration of RO_2• at the surface of small ML/MH particles. On the other hand, at the higher light-intensity region, the probability of accumulation of four electrons in one particle can be assumed, and it is expected that the order of light-intensity dependence for this absorption to create <BWO(4e)> is four. If higher-order light-intensity dependence at the highest intensity region is presumed for FB and 500FB (**Fig. 6**), the dependence is attributable to the four-electron reduction of O_2 and higher probability of those large particles to absorb multiple photons.

4. Conclusions

The rate of photocatalytic CO_2 liberation from a BWO-suspended aqueous acetic-acid solution under monochromatic irradiation with a grating-type monochromator or a high-intensity UV LED depended strongly on the structural/physical properties of BWO samples. The observed light-intensity dependence of the photocatalytic reaction rates was generally bimodal, i.e., the

light-intensity dependence could be simulated by assuming first order and 0.5th order in lower and higher light-intensity ranges. The observed bimodal light-intensity dependence could be reproduced by a presumed kinetic model including multielectron reduction of O_2 induced by accumulation of two photoexcited electrons in one photocatalyst particle and subsequent radical chain reaction with peroxy radicals as chain carriers to complete oxidative acetic-acid decomposition. In the presumed mechanism, the probability of accumulation of two electrons in one photocatalyst particles is increased in proportion to the square of light intensity, i.e., I^2, (The square-root term due to the second-order rate of termination reaction in the radical chain mechanism leads to first-order light-intensity dependence in total.) at a lower intensity range, while at higher intensity, the two-electron accumulation is guaranteed to result in 0.5th-order light-intensity dependence. The calculated threshold intensity, I_{thr}, at which the order was formally changed from 1 to 0.5 depended also on the structural/physical properties of BWO samples. The results, for example, the lower I_{thr} of FB-BWO with higher activity than that of ML and MH-BWOs and the similar I_{thr} of calcined 500FB-BWO with activity which was similar to that of FB-BWO, are attributable to preferable two-electron accumulation in larger crystallites or crystal aggregates.

It has commonly been believed in the field of photocatalysis that dependence of photocatalytic activities on structural/physical properties of photocatalyst particles is attributable to differences in, for example, the amount of adsorbed substrate(s) on the surface of photocatalyst particles, rate of electron/positive hole transfer, and/or rate of their recombination. The results presented in this paper provide a novel insight, for the first time to the authors' knowledge (Secondary particle size-dependent photocatalytic activity was speculated in statistical studies [20,21].), that the observed structural/physical properties-dependent photocatalytic activities can also be interpreted by the difference in light-intensity dependence; the larger the effective size of photocatalyst particles is, the higher is their photocatalytic activity, especially for photocatalytic systems in which multielectron/positive hole transfer is included. Thus, kinetic studies on heterogeneous photocatalysis based on light intensity-dependence measurements may be a unique and effective way for exploring the intrinsic mechanism of heterogeneous photocatalysis. Study along this line is now in progress.

Acknowledgements

FE-SEM analyses of samples were carried out using a JEOL JSM-7400F electron microscope at the Open Facility, Hokkaido University Sousei Hall. This work was partly supported by Grant-in-Aid for Challenging Exploratory Research (KAKENHI) from the Japan Society for the Promotion of Science (JSPS) (16K1408606).

References

[1] B. Ohtani, Principle of photocatalysis and design of active photocatalysts, in: S. Suib (Ed.), Solar Photocatalysis, Elsevier, Amsterdam, The Netherlands, 2013, pp.121–144.

[2] B. Ohtani, Design and development of active titania and related photocatalysts, in: P. Pichat (Ed.), Photocatalysis and Water Purification: From Fundamentals to Recent Application, Wiley-VCH, Verlag Berlin, 2013, pp.75–102.

[3] K. Nakata, A. Fujishima, J. Photochem. Photobiol. C Photochem. Rev. 13 (2012) 169–189.

[4] V. Augugliaro, M. Bellardita, V. Loddo, G. Palmisano, L. Palmisano, S. Yurdakal, J. Photochem. Photobiol. C Photochem. Rev. 13 (2012) 224–245.

[5] D. E. Scaife, Sol. Energy 25 (1980) 41–54.

[6] B. Ohtani, Electrochemistry 82 (2014) 414–425.

[7] H. Hori, M. Takashima, M. Takase, B. Ohtani, Chem. Lett. 46 (2017) 1376–1378.

[8] H. Hori, M. Takashima, M. Takase, M. Kitamura, F. Amano, B. Ohtani, Catal. Today 303 (2018) 341–349.

[9] H. Fu, L. Zhang, W. Yao, Y. Zhu, Appl. Catal. B: Environ. 66 (2006) 100–110.

[10] T. Saison, P. Gras, N. Chemin, C. Chaneac, O. Durupthy, V. Brezova, C. Colbeau-Justin, J.-P. Jolivet, J. Phys. Chem. C 117 (2013) 22656–22666.

[11] R. Abe, H. Takami, N. Murakami, B. Ohtani, J. Am. Chem. Soc. 130 (2008) 7780–7781.

[12] Y. Kim, H. Irie, K. Hashimoto, Appl. Phys. Lett. 92 (2008) 182107.

[13] T. Arai, M. Yanagida Y. Konishi, Y. Iwasaki, H Sugihara, K. Sayama, Catal. Commun. 9 (2008) 1254–1258.

[14] H. Irie, S Miura, K. Kamiya, K Hashimoto, Chem. Phys. Lett. 457 (2008) 202–205.

[15] A. J. Bard, R. Parsons, J. Jordan, Standard Potentials in Aqueous Solution, Marcel Dekker, New York and Basel, 1985.

[16] J. Sheng, X. Li, Yiming Xu, ACS Catal. 4 (2014) 732−737.

[17] F. Amano, K. Nogami, R. Abe, B. Ohtani, J. Phys. Chem. C 112 (2008) 9320–9326.

[18] H. Hori, M. Takase, M. Takashima, F. Amano, T. Shibayama, B. Ohtani, Catal. Today 300 (2017) 99–111.

[19] H. Hori, M. Takase, F. Amano, B. Ohtani, Chem. Lett. 44 (2015) 1723–1725.

[20] O.-O. Prieto-Mahaney, N. Murakami, R. Abe, B. Ohtani, Chem. Lett. 38 (2009) 238–239.

[21] B. Ohtani, O.-O. Prieto-Mahaney, F. Amano, N. Murakami, R. Abe, J. Adv. Oxid. Technol. 13 (2010) 247–261.

[22] F. Amano, K. Nogami, B. Ohtani, J. Phys. Chem. C 113 (2009) 1536–1542.

[23] B. Ohtani, J. Photochem. Photobiol. C Photochem. Rev. 11 (2010) 157–178.

[24] B. Ohtani, Phys. Chem. Chem. Phys. 16 (2014) 1788–1797.

[25] S. Kato, F. Masuo, Kogyo Kagaku Zasshi 67 (1964) 1136–1140.

[26] Y. Ohko, D. A. Tryk, K. Hashimoto, A. Fujishima, J. Phys. Chem. B 102 (1998) 2699–2704.

[27] T. Torimoto, Y. Aburakawa, Y. Kawahara, S. Ikeda, B. Ohtani, Chem. Phys. Lett. 392 (2004) 220–224.

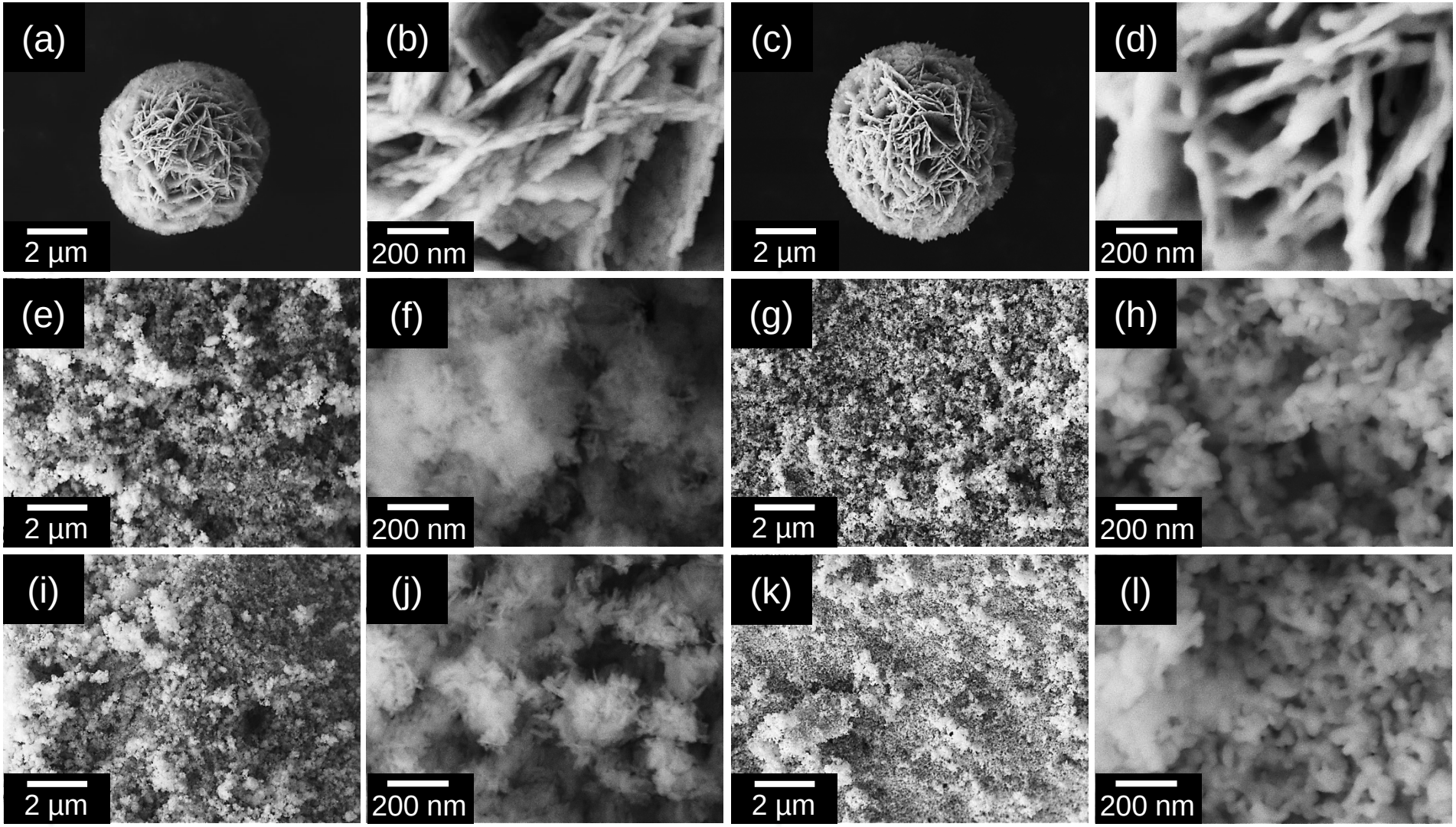
(a)
2 µm
(b)
200 nm
(c)
2 µm
(d)
200 nm
(e)
2 µm
(f)
200 nm
(g)
2 µm
(h)
200 nm
(i)
2 µm
(j)
200 nm
(k)
2 µm
(l)
200 nm

Fig. 1

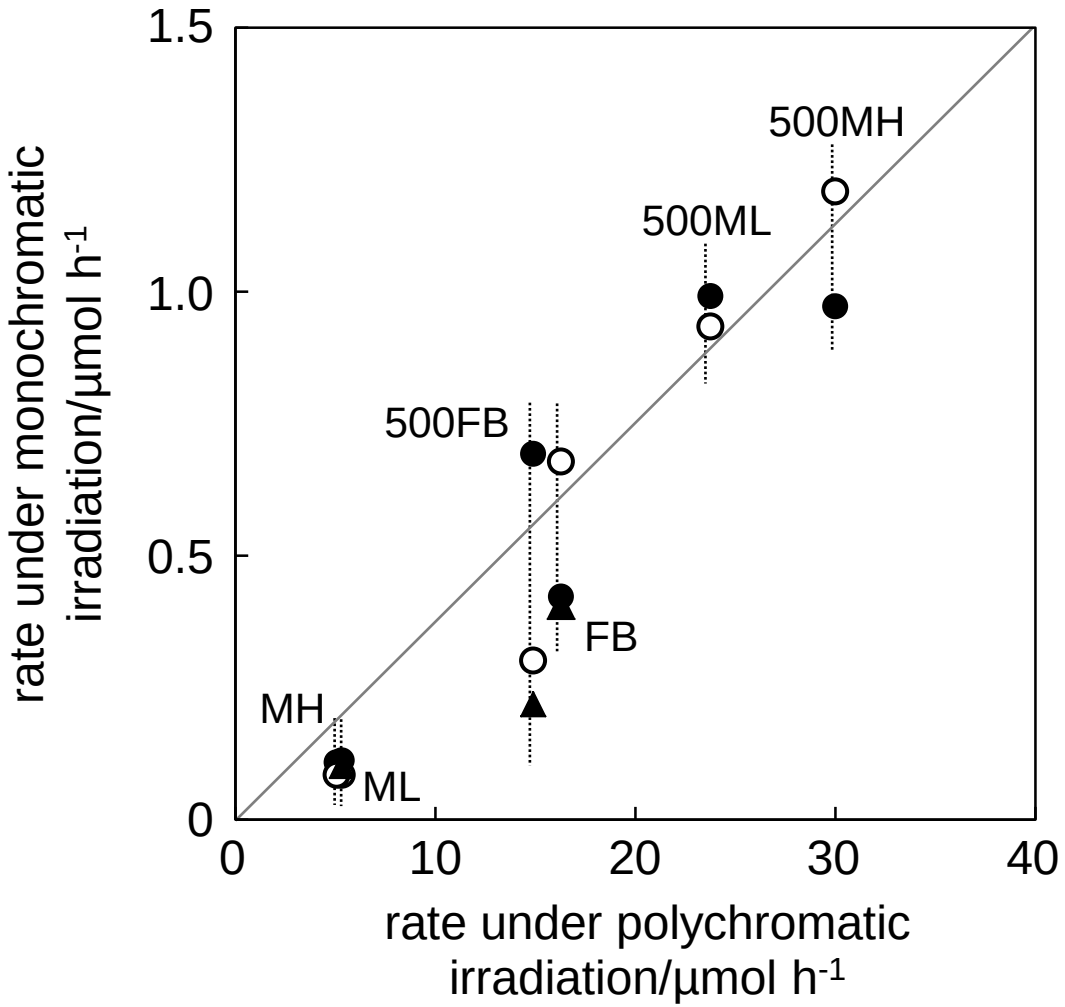
1.5
1.0
0.5
0
0
10
20
30
40
500MH
500ML
500FB
FB
MH
ML
rate under monochromatic irradiation/μmol h-1
rate under polychromatic irradiation/μmol h-1

Fig. 2

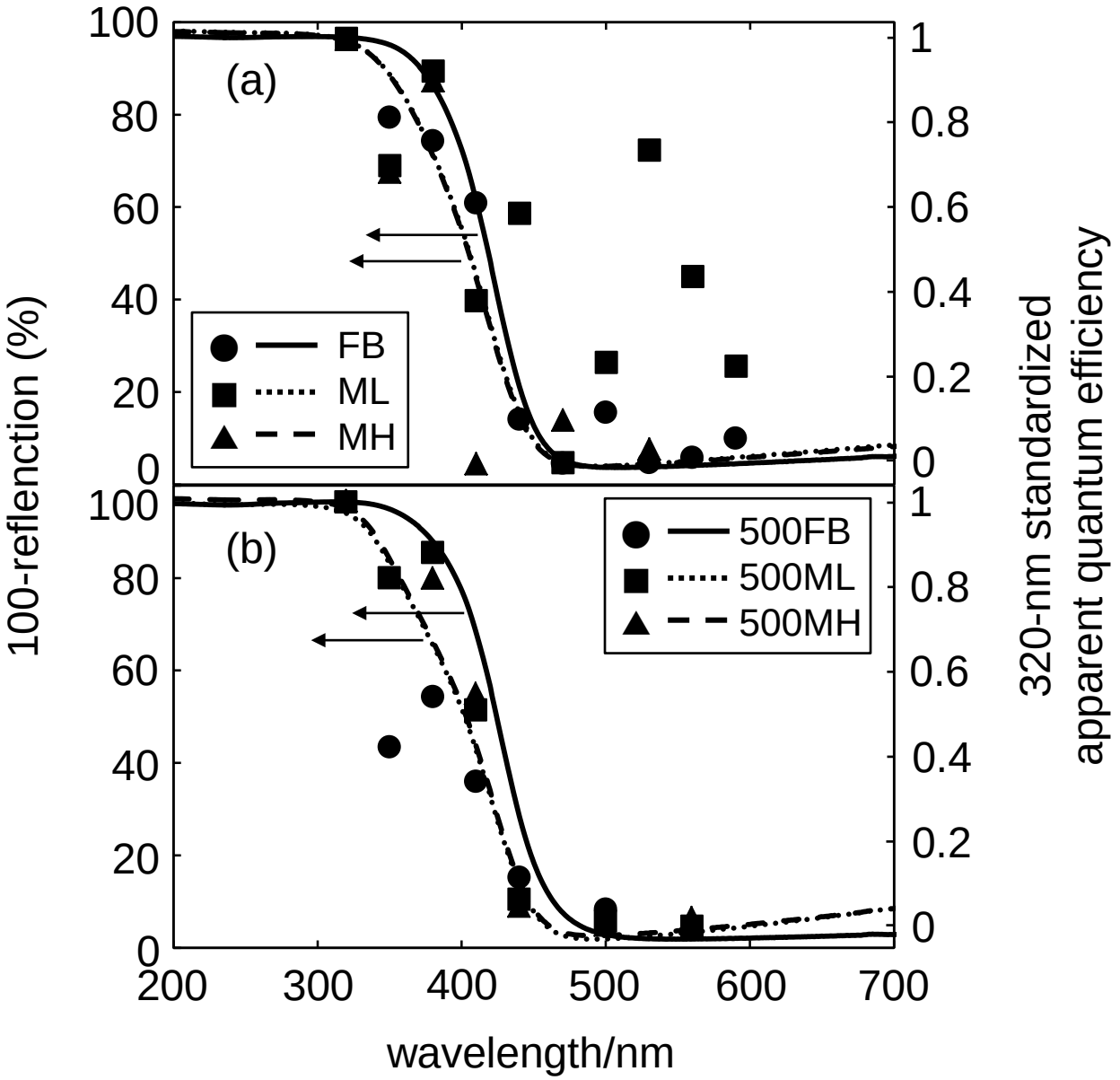
100
80
60
40
20
0
(a)
FB
ML
MH
1
0.8
0.6
0.4
0.2
0
100-reflenction (%)
(b)
500FB
500ML
500MH
200
300
400
500
600
700
wavelength/nm
320-nm standardized
apparent quantum efficiency

Fig. 3

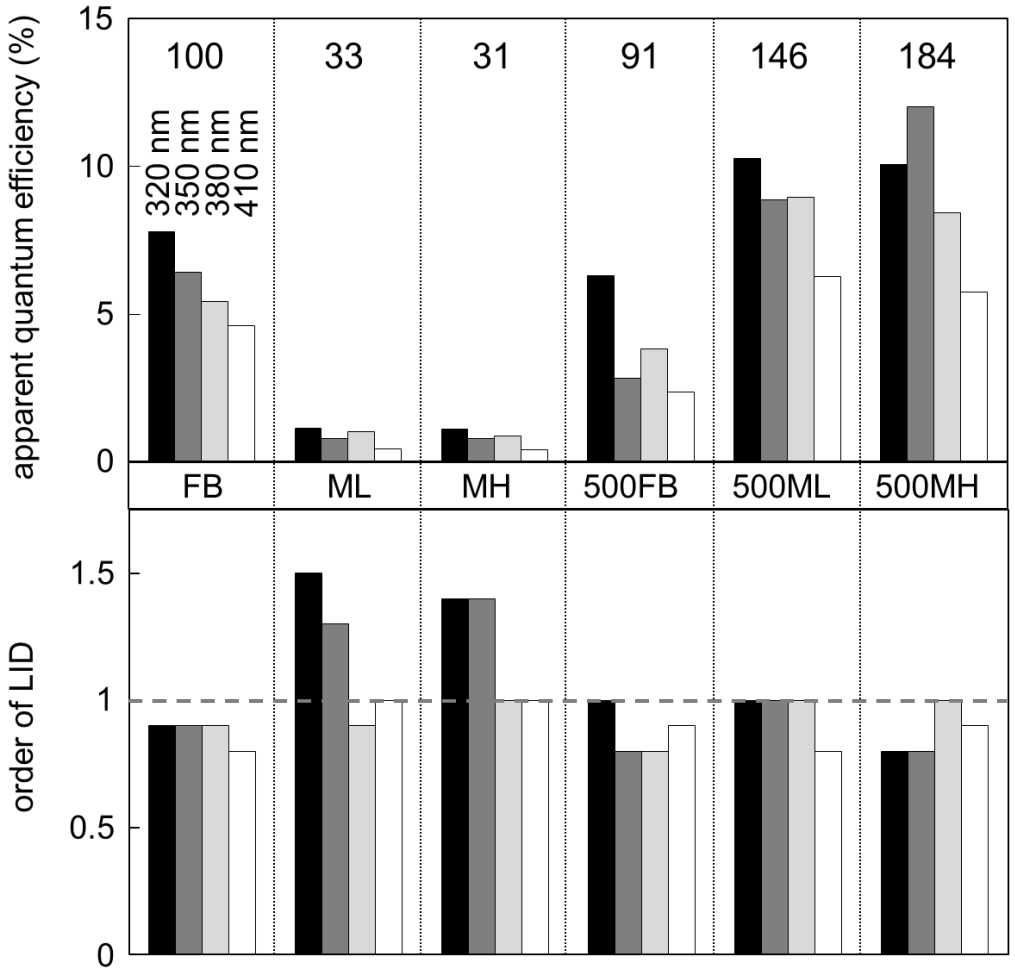
apparent quantum efficiency (%)
15
10
5
0
100
33
31
91
146
184
320 nm
350 nm
380 nm
410 nm
FB
ML
MH
500FB
500ML
500MH
order of LID
1.5
1
0.5
0

Fig. 4

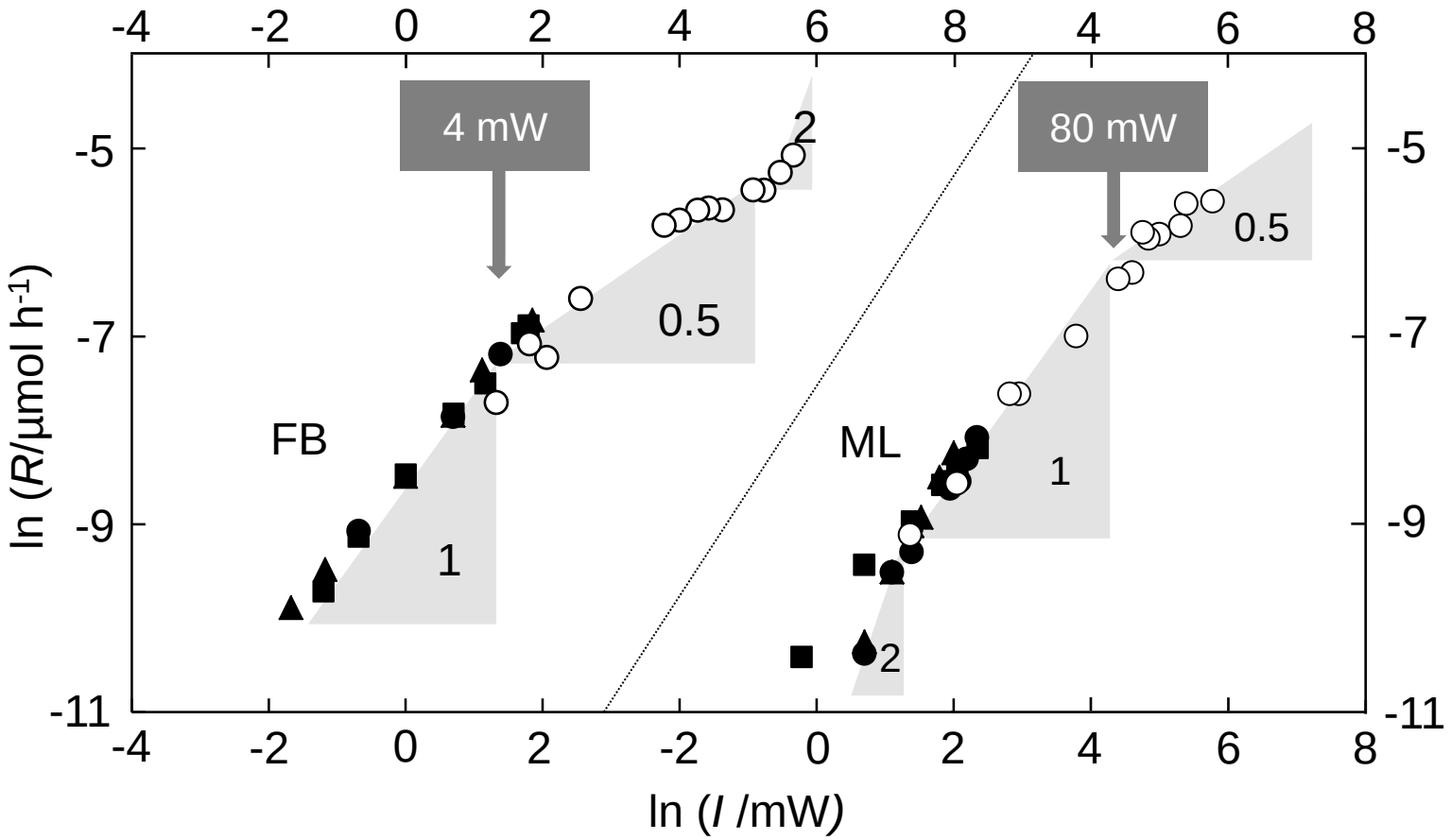

Fig. 5

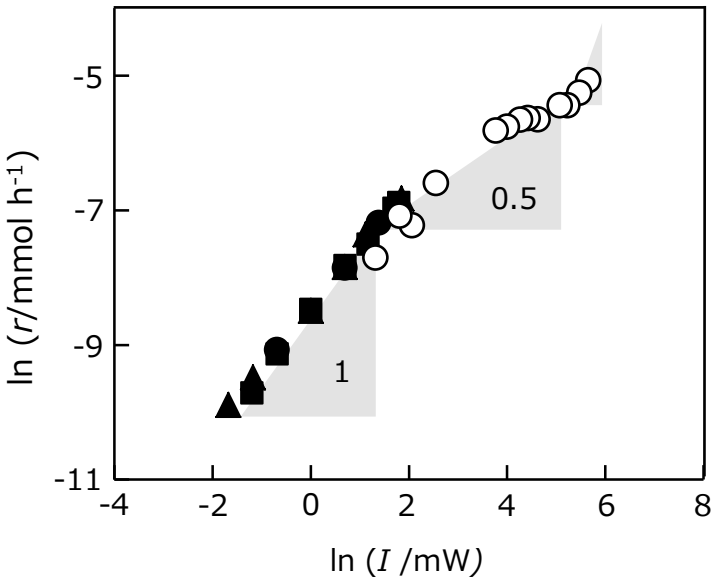
-5
-7
-9
-11
-4
-2
0
2
4
6
8
ln (r/mmol h-1)
ln (I /mW)
0.5
1

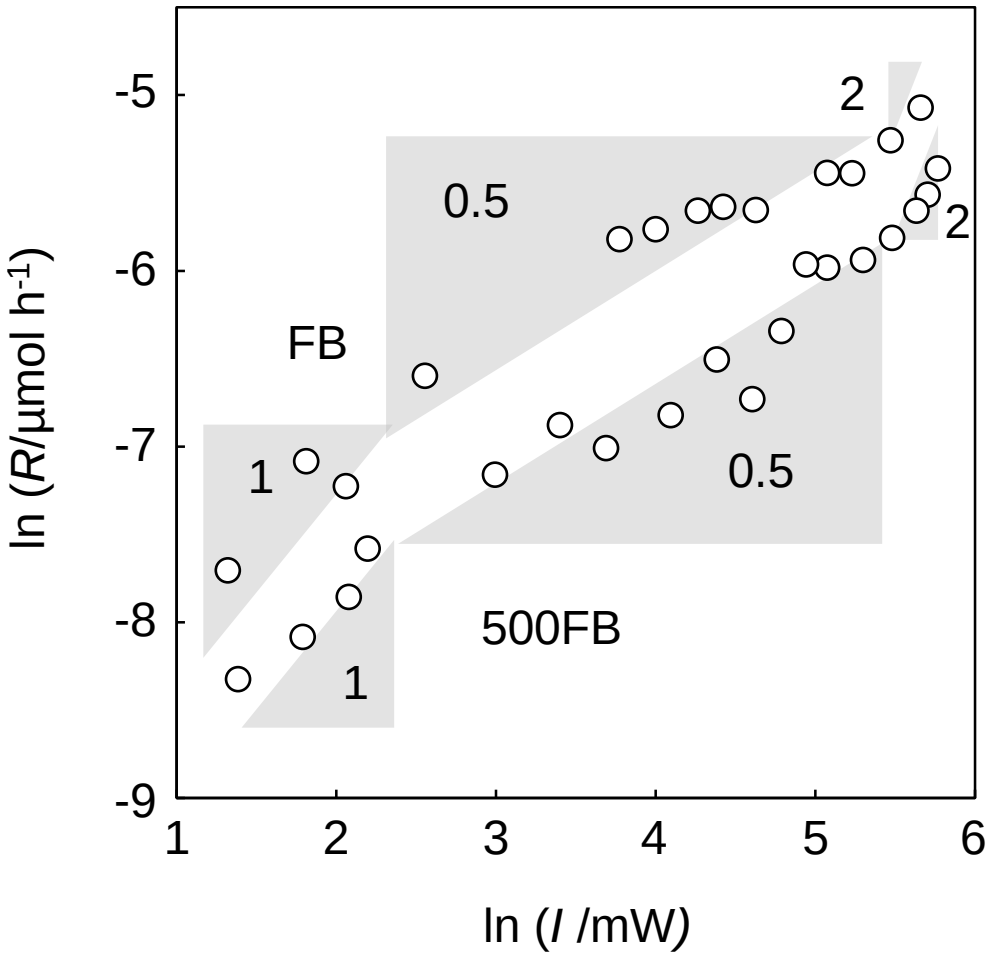

Fig. 6